



AIAA 2002-0929

Numerical Analysis of 1st and 2nd Cycles of Oxyhydrogen PDE

S. Kawai and T. Fujiwara
Department of Aerospace Engineering
Nagoya University, Nagoya, JAPAN

40th Aerospace Sciences Meeting & Exhibit
14–17 January 2002
Reno, Nevada

NUMERICAL ANALYSIS OF 1ST AND 2ND CYCLES OF OXYHYDROGEN PDE

Soshi KAWAI* and Toshi FUJIWARA†

Department of Aerospace Engineering, Nagoya University,
Nagoya 464-8603, Japan

Abstract

One-dimensional analyses of pulse detonation engine (PDE) have been performed by numerous workers without considering injection phase. 1-D codes have fundamental defects in considering transport processes (viscosity, heat conductivity and diffusion) and injection phase. In studying PDE, a key issue would be how to generate a CJ/quasi-CJ detonation in a short distance. Therefore, investigation of injection and ignition has become unavoidable.

In the present analysis, the performance of straight single Model PDEs having various tube lengths is studied; for combustion phase, exhausting phase and injection phase, using two-dimensional unsteady calculations, where we used a MacCormack-TVD numerical scheme to solve Navier-Stokes equations.

Introduction

A detonation phenomenon is the interaction between front-running shock wave and subsequent coupled combustion, generating a high pressure and temperature which is basically uncontrollable in comparison with conventional flames. The direction of research has mostly been prevention of or protection from hazard.

Since several years ago, however, there has occurred a trend to control detonation propagation, and to utilize its high power and high-density energy in positive

directions like pulse detonation engine (PDE)^[1]; Eidelman et al. reignited the study of PDE. Pulse detonation engine research has widely spread out recently, because it is considered as a good candidate for aerospace propulsion system of next generation^[2].

In the present work, a 2-dimensional cycle analysis of PDE containing an Ar-diluted stoichiometric oxyhydrogen mixture is performed. To achieve a "high-frequency-running" engine, we pay attention specifically to the exhausting and injection process during the 2nd cycle, where the burnt gas generated in the 1st cycle still remains within the detonation tube. A 2nd-order MacCormack-TVD scheme is used to solve Navier-Stokes equations where a simplified two-step chemical reaction model^[3] is introduced.

Physical Model and Numerical Method

The governing equations are two-dimensional Navier-Stokes ones, containing the mass conservation equations for two progress variables α (induction reaction) and β (exothermic reaction).

$$\frac{\partial \mathbf{U}}{\partial t} + \frac{\partial \mathbf{E}}{\partial x} + \frac{\partial \mathbf{F}}{\partial y} = \frac{\partial \mathbf{E}_\nu}{\partial x} + \frac{\partial \mathbf{F}_\nu}{\partial y} + \mathbf{S} \quad (1)$$

$$\mathbf{U} = \begin{pmatrix} \rho \\ \rho u \\ \rho v \\ e \\ \rho \beta \\ \rho \alpha \end{pmatrix}, \mathbf{E} = \begin{pmatrix} \rho u \\ \rho u^2 + p \\ \rho uv \\ (e + p)u \\ \rho \beta u \\ \rho \alpha u \end{pmatrix}, \mathbf{F} = \begin{pmatrix} \rho v \\ \rho uv \\ \rho v^2 + p \\ (e + p)v \\ \rho \beta v \\ \rho \alpha v \end{pmatrix},$$

$$\mathbf{E}_\nu = \begin{pmatrix} 0 \\ \tau_{xx} \\ \tau_{xy} \\ u\tau_{xx} + v\tau_{xy} - q_x \\ \rho D_\beta \frac{\partial \beta}{\partial x} \\ 0 \end{pmatrix},$$

*Graduate student, AIAA student member
Email: soukun@momo.nuae.nagoya-u.ac.jp

†Professor

Copyright©2001 by the American Institute of
Aeronautics and Astronautics. Inc.
All rights reserved

$$\mathbf{F}_\nu = \begin{pmatrix} 0 \\ \tau_{yx} \\ \tau_{yy} \\ u\tau_{yx} + v\tau_{yy} - q_y \\ \rho D_\beta \frac{\partial \beta}{\partial y} \\ 0 \end{pmatrix}, \mathbf{S} = \begin{pmatrix} 0 \\ 0 \\ 0 \\ 0 \\ \rho w_\beta \\ \rho w_\alpha \end{pmatrix}$$

In the modified Korobeinikov-Levin chemical model, the rate constants are adjusted to agree, regarding its chemical induction time and temperature profile, with Oran's elementary reaction model^[4] as much as possible. The two progress variables α and β are explicitly given in the following:

α (induction reaction)

$$w_\alpha \equiv \frac{d\alpha}{dt} = -\frac{1}{\tau_{ind}} = -k_1 \rho \exp\left(-\frac{E_1}{RT}\right)$$

β (exothermic reaction)

$$w_\beta \equiv \frac{d\beta}{dt} = \begin{cases} 0 & (\alpha > 0) \\ -k_2 p^2 \left\{ \beta^2 \exp\left(-\frac{E_2}{RT}\right) \right. \\ \left. -(1-\beta)^2 \exp\left(-\frac{E_2+q}{RT}\right) \right\} & (\alpha \leq 0) \end{cases}$$

The present Model PDE is a straight 2-D detonation channel with its upstream end closed, having ports to inject an oxyhydrogen mixture ($2\text{H}_2 + \text{O}_2 + 7\text{Ar}$), while the downstream end is open for exhausting a burnt gas. Our PDE runs under the ground condition at $P_{env}=1.0\text{atm}$. Since calculation domain is only inside PDE, the influence of environment comes into play only through the pressure at tube end for subsonic flow conditions. The PDE wall is assumed adiabatic and non-catalytic, as shown in Fig.1. The computations are performed for 4 different PDE lengths as listed in Table1.

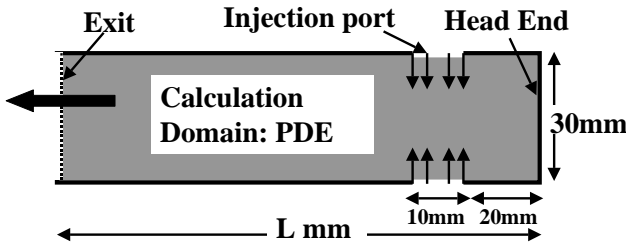


Fig. 1: Calculation domain of Model PDE

Resolution/Mesh Convergence

It is known in numerical analysis of detonation that the physical properties obtained from calculation are

Table 1: Model PDE configuration

Case	PDE width [mm]	PDE length (L [mm])
a	30.0	100.0
b	30.0	200.0
c	30.0	300.0
d	30.0	400.0

highly dependent on the grid resolution and numerical scheme. The resolution is upgraded as much as possible, by testing 3 different grids. The effect of grid resolution on cell size is shown in Table2 at the initial pressure 0.5atm and temperature 298.15K, which yielded the experimental cell size $\lambda=0.49\text{cm}$ according to Strehlow^[6]. As seen in Table2, the cell size does not change when the mesh size gets less than $100\mu\text{m}$. Furthermore, in comparison with the experimental cell size $\lambda=0.49\text{cm}$, both Grid2 and Grid3 give $\lambda=0.6\text{cm}$ ($1.22 \times$ experimental λ), reasonably close to the experimental cell size. Thus, we can conclude that Grid1's resolution is not enough while Grid2 and Grid3 are reliable, giving mesh convergence. Based upon these results, the present analyses are carried out using Grid2 where the mesh size is $100\mu\text{m}$. The grid number is $(L \times 10) \times 300$ ($\Delta x = \Delta y = 100\mu\text{m}$). It has turned out that the present grid number is sufficient for PDE cycle analysis, but not for the detailed behaviors of boundary layer.

Table 2: Effect of resolution on calculated cell size

	Mesh size [μm]	Cell size [cm]	Ratio between calculated and experimental cell sizes
grid1	150.0	0.75	1.53
grid2	100.0	0.6	1.22
grid3	67.0	0.6	1.22

Results and Discussion

Numerical Analysis of 1st Cycle

Combustion Process

In this analysis, the 1st cycle starts after an oxyhydrogen mixture is filled up in the 2-D channel of 30mm width and various lengths L under the initial pressure $P_0=1.00\text{atm}$ and temperature $T_0=298.15\text{K}$.

Ignition in 1st cycle has already been performed by assuming a CJ detonation obtained from 1-D analysis. In order to generate a 2-dimensional detonation,

the initial 1-D detonation starting from the closed upstream end is disturbed by placing inhomogeneities near wall, which act like a Shchelkin wire. The 1-D CJ detonation is perturbed into a 2-D detonation in a short "DDT distance", propagating toward downstream end. Thereafter, the 2-D detonation front leaves the channel, followed by burnt gas exhaust from channel; at the instant when the head-end pressure $P_h = P_{env} (= 1.0 \text{ atm})$, the fresh mixture starts flowing from the injection ports into the 2nd cycle. The propagation velocity of detonation front is shown in Fig.2, where the calculated velocity during 100mm traveling (Case(a)) during 1st cycle is found close to the CJ value. In addition, there is essentially no difference among 4 Cases under consideration. The pressure distribution snapshot (Case(a)) and distribution of pressure and temperature (Case(a)) along PDE center axis, at the instant when detonation front has reached PDE exit ($56.2 \mu\text{sec}$ after ignition), are shown in Fig.3 and Fig.4. Fig.5 shows the change of pressure distribution along PDE (Case(a)) center axis during evolution of combustion process after ignition.

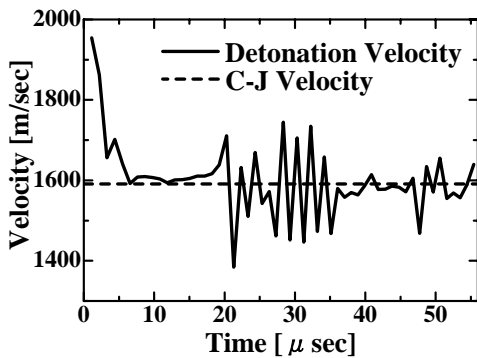


Fig. 2: Temporal variation of detonation velocity

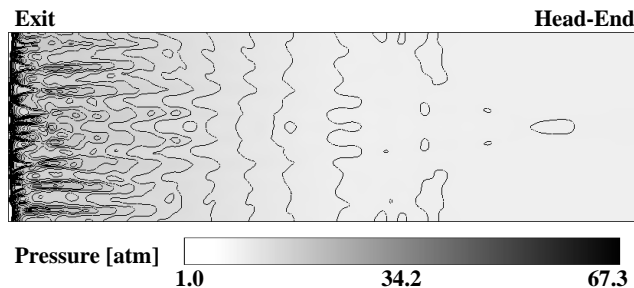


Fig. 3: Pressure contour (Case(a)) at instant when detonation front has reached exit

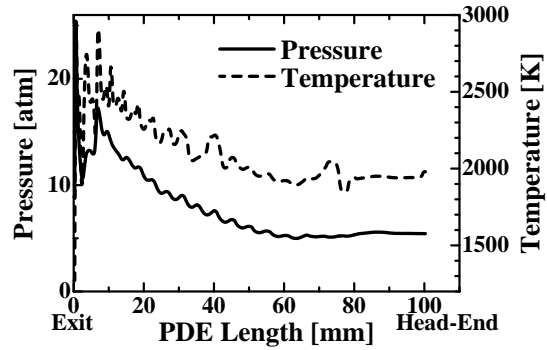


Fig. 4: Distribution of pressure and temperature (Case(a)) along PDE center axis

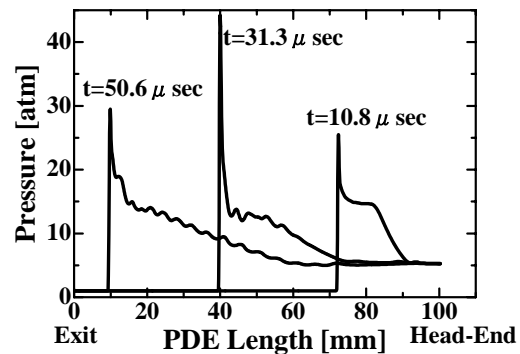


Fig. 5: Combustion evolution along PDE (Case(a)) center axis after ignition

Exhaust of Combustion Products

The boundary condition utilized at open end is derived from the method of characteristics. This ensures no constraints imposed on the flow quantities when the outflow is supersonic, whereas it enforces the required constraints when the flow becomes subsonic.

The history of pressure and temperature at the center of intake port and head-end, until immediately before the fresh oxyhydrogen intake ports are opened up, is shown in Fig.6 and Fig.7. At this valve opening time, the head-end pressure is equal to the environment pressure ($P_h = P_{env} = 1.0 \text{ atm}$). By the time when fuel injection starts from intake ports, the pressure at intake ports has become 0.98 atm while the temperature is kept at 1270 K . Since the detonation velocity is very close to CJ velocity $U = 1591 \text{ m/sec}$, the time for the detonation to leave the length 100 mm (Case(a)) is $t = 56.2 \mu\text{sec}$; at $t \leq 56.2 \mu\text{sec}$, therefore, the detonation front is still barely inside the channel. Fig.6 indicates that the pressure history can be divided into two distinct stages, as pointed out by Kailasanath^[5];

(1) arrival of shock immediately after ignition and (2) a plateau at $t \geq 17 \mu\text{sec}$. The plateau pressure $P_p/P_{cj} = 0.38$, i.e. $P_p = 5.27 \text{ atm}$ ($P_{cj} = 13.86 \text{ atm}$) lasts for a long time $17 \mu\text{sec} \leq t \leq 171 \mu\text{sec}$, followed by (3) the relaxation $171 \mu\text{sec} \leq t \leq 367 \mu\text{sec}$ down to a low pressure $P_h/P_{env} = 1$. This plateau pressure is the primary part to generate thrust. Fig.8 gives the history of Mach number at the center of exit plane. With regard to the flow at exit plane, its Mach number is kept always at 1.0 from the start of exhaust until $259.1 \mu\text{sec}$ later, indicating that the exit flow is choked. Thereafter, the flow at exit plane decreases down to subsonic.

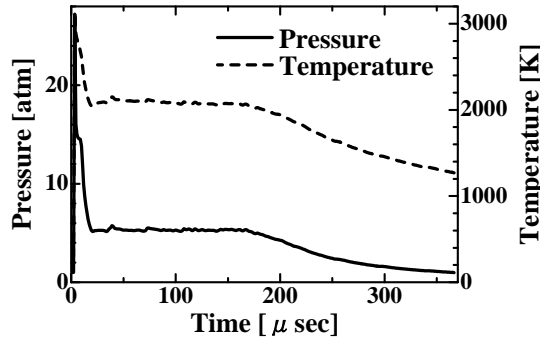


Fig. 6: Evolution of pressure and temperature at center of intake port (Case(a))

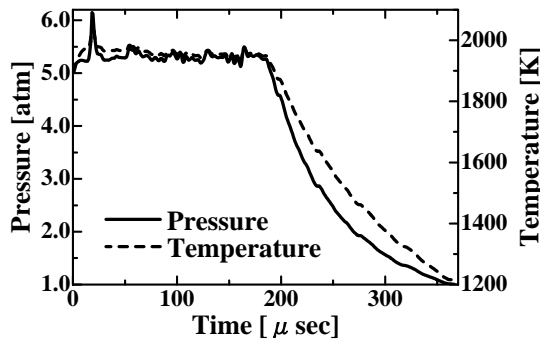


Fig. 7: Evolution of pressure and temperature at head-end (Case(a))

The pressure distribution snapshot (Case(a)) and the distribution of pressure and temperature (Case(a)) along PDE center axis, at the instant immediately before the fresh oxyhydrogen intake ports are opened up ($367.1 \mu\text{sec}$ after ignition, and $P_h = P_{env} = 1.0 \text{ atm}$), are shown in Fig.9 and Fig.10. Fig.11 shows the change of pressure distribution along center axis, at several times during the pressure relaxation process in PDE (Case(a)); the time is now counted from the start of exhaust. Fig.11 indicates that the burnt gas from the

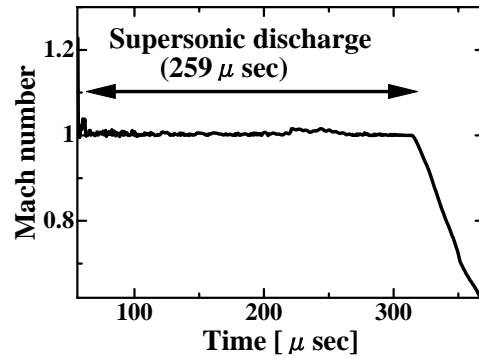


Fig. 8: Evolution of Mach number at center of exit (Case(a))

1st cycle exhausts quickly from open the end, where the pressure decrease in PDE is influenced by the environmental pressure.

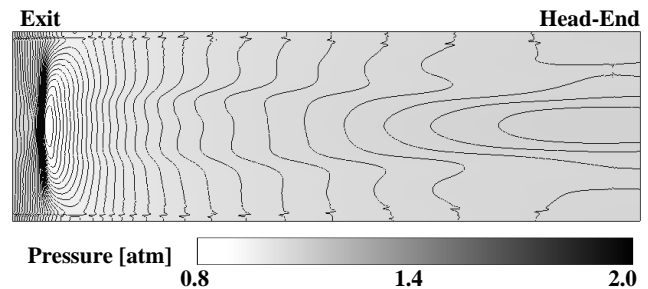


Fig. 9: Pressure contour (Case(a)) immediately before fresh oxyhydrogen intake ports are opened up.

Next, the specific impulse is estimated from the history of head-end pressure P_h minus environmental pressure P_{env} ($=1.0 \text{ atm}$), as follows:

$$\begin{aligned}
 I_{sp} &= \frac{[\text{Impulse per unit length during 1 cycle}]}{[\text{Filled fuel mass per unit length}]} \\
 &= \frac{\int_0^W \int_0^{t_{env}} (P_h - P_{env}) dy dt}{\int_0^W \int_0^L \rho_0 g dy dx} \quad (2)
 \end{aligned}$$

where ρ_0 denotes the filled fuel density, and t_{env} the time elapsed until $P_h = P_{env}$ is realized.

The specific impulse I_{sp} for 4 Cases acquired from Formula (2) is shown in Table3. Although a slightly increasing tendency of specific impulse is seen for longer tubes, we can derive a general conclusion that I_{sp} is irrelevant to PDE length as long as DDT distance is assumed zero.

The temporal behavior of impulse (Case(a)) per unit depth is shown in Fig.12; the asymptotic limit of im-

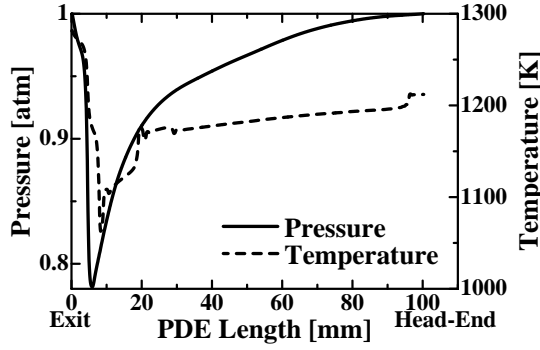


Fig. 10: Distribution of pressure and temperature (Case(a)) along PDE center axis, at the instant when oxyhydrogen intake ports are opened up.

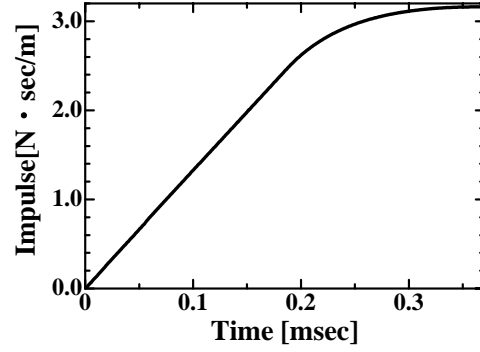


Fig. 12: Evolution of impulse per unit depth (Case(a))

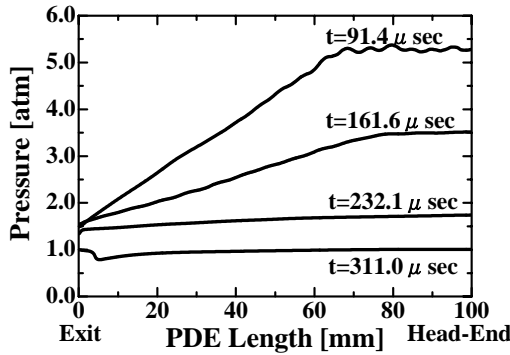


Fig. 11: Pressure relaxation process along PDE (Case(a)) center axis.

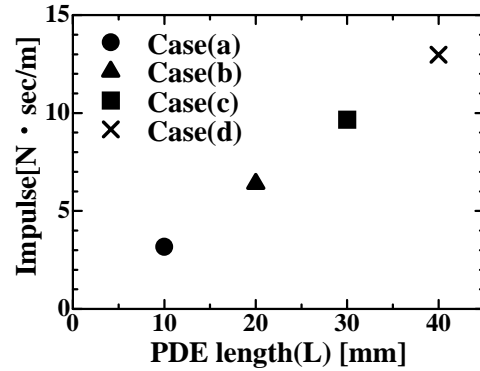


Fig. 13: Impulse compared among 4 Model PDEs (Cases(a)~(d))

pulse (Case(a)) is set to 3.16 [N·sec/m] to define the one-cycle time t_{env} . Note here that the impulse per unit depth is proportional to PDE length (L), as shown in Fig.13.

Next, we try to compare the results of numerical analysis, using a figure on impulse per unit area, first proposed by Kailasanath on the basis of 1-D numerical analysis, as is shown in Fig.14. The impulse obtained by Kailasanath 1-D analysis is proportional to the product of t_{CJ} defined by $L(\text{PDE length})/D_{CJ}$ and the pressure difference $P_p - P_{env}$, where D_{CJ} is the CJ velocity. Interestingly, our results of 2-dimensional analysis also come onto the same straight line.

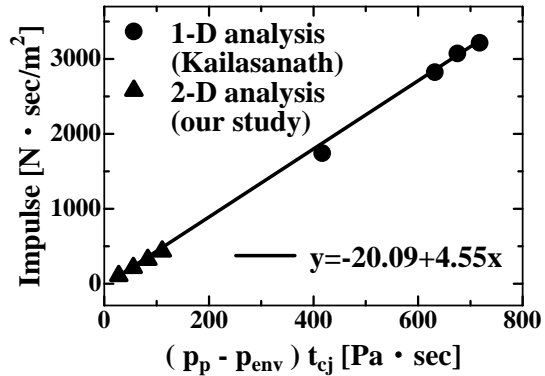


Fig. 14: Impulse curve of Kailasanath 1-D analysis compared with our 2-D results

Table 3: Specific impulse I_{sp} for 4 Cases

Case	a	b	c	d
$I_{sp}[\text{sec}]$	6576	6651	6702	6747

Numerical Analysis of 2nd Cycle

Injection

Immediately after the head-end pressure P_h has decreased down to the environmental pressure P_{env} , a fresh oxyhydrogen mixture is injected into PDE, that still contains a high-temperature burnt gas, by opening the intake ports.

Size effect of intake port is tested, by locating the port specifically at the center of PDE head-end, where the open ratio=intake port width/PDE width=1.0-0.17 with the port connected to a reservoir tank of $P_r=10.0\text{atm}$ and $T_r=298.15\text{K}$; the inflow Mach number is set to 1.0. The pressure and temperature around intake port is $P_i=1.00\text{atm}$ and $T_i=1212\text{K}$. The relation between calculated fuel injection time and open ratio is shown in Fig.15; when the open ratio becomes smaller, the fuel injection time sharply increases, indicating the existence of proper value.

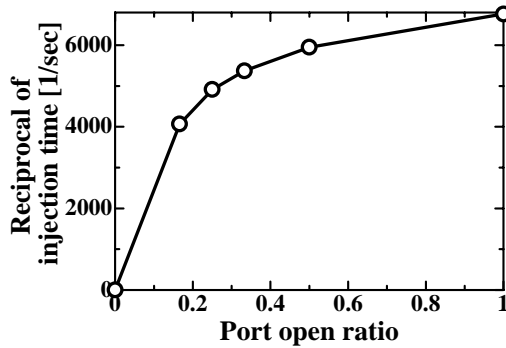


Fig. 15: Relation between calculated injection time and port open ratio

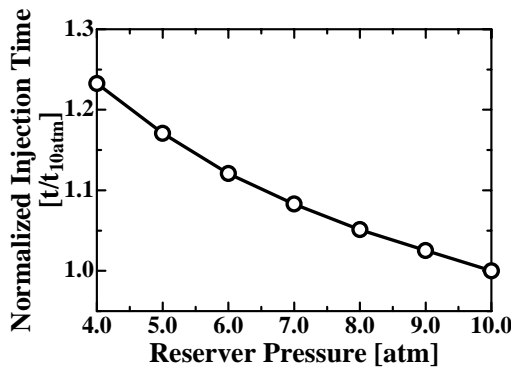


Fig. 16: Relation between calculated injection time and reservoir pressure

Next, the effect of reservoir pressure is tested for a Model PDE (Case(a)) as shown in Fig.1. Normalized

fuel injection time (injection time/injection time for reservoir pressure 10atm) for different reservoir pressures in Case(a) is compared, where the reservoir pressure P_r is changed between 10 to 4atm. Fig.16 shows that the calculated fuel injection time is a decreasing function of the reservoir pressure, as is easily expected; the difference is only 25% for the pressure change $P_r=10\text{-}4\text{atm}$. We performed an analysis to find out dependence of injection angle on fuel injection time; no influence is seen to fuel injection time. In conclusion, the fuel injection time depends on (1) intake port width and (2) reservoir pressure P_r .

Henceforth, the fuel injection time is studied for 4 Cases of Model PDE connected to the $P_r=10.0\text{atm}$ reservoir tank at $T_r=298.15\text{K}$ (fuel injection is right-angled to wall), where the performance of 4 Model PDEs are also calculated. The inflow Mach number is kept at 1.0. The β distribution in PDE (Case(a)) at 61.4, 96.3, and 153.8 μsec after start of injection is shown in Fig.17. By injecting an oxyhydrogen mixture from intake ports during the 2nd cycle, the expansion and diffusion of fuel are observed. The distribution of β along PDE (Case(a)) center axis after the start of fuel injection is shown in Fig.18; β is about 1.0 (unburnt mixture) nearly everywhere in PDE behind the contact surface. The features of fuel injection can be understood from Fig.17 and Fig.18.

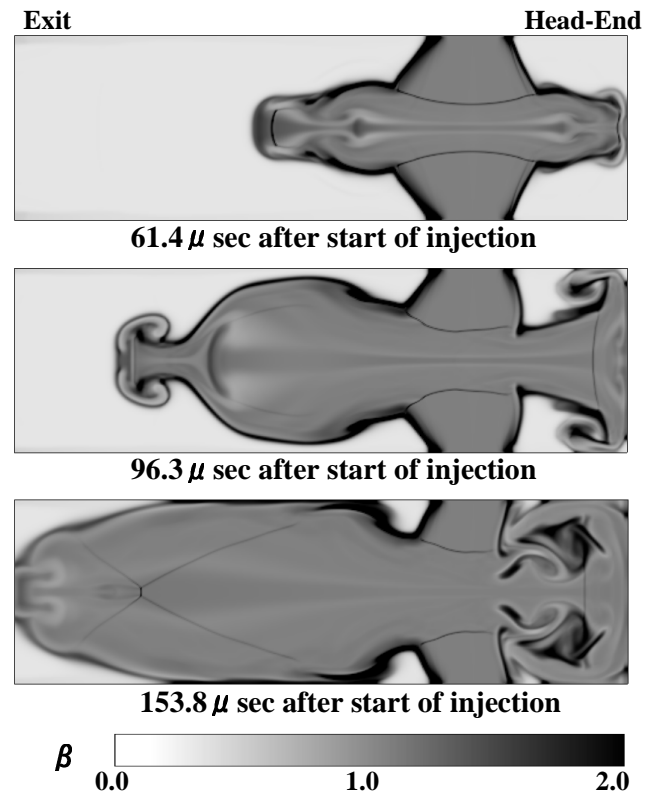


Fig. 17: β distribution in PDE (Case(a)) after start of fuel injection

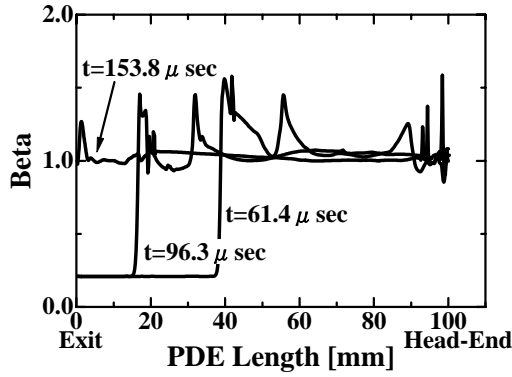


Fig. 18: Distribution of β along PDE (Case(a)) center axis at different times after start of injection

Table 4: Time for each process in one cycle for 4 Model PDEs (Cases(a)~(d))

Case	a		b	
	[sec]	[%]	[sec]	[%]
Combustion	5.62×10^{-5}	10.8	1.20×10^{-4}	11.0
Exhausting	3.31×10^{-4}	59.7	6.27×10^{-4}	57.4
Injection	1.54×10^{-4}	29.5	3.46×10^{-4}	31.6
1 Cycle	5.21×10^{-4}	100	1.09×10^{-3}	100
Case	c		d	
	[sec]	[%]	[sec]	[%]
Combustion	1.84×10^{-4}	11.1	2.47×10^{-4}	11.1
Exhausting	9.51×10^{-4}	57.5	1.29×10^{-3}	58.0
Injection	5.19×10^{-4}	31.4	6.88×10^{-4}	30.9
1 Cycle	1.65×10^{-3}	100	2.22×10^{-3}	100

The time required for combustion, exhaust, fuel injection, and cycle completion for Cases(a) through (d) is shown in Table4. The ratio between each process and complete cycle is also shown as % in Table4. As another representation of Table4, a bar graph on percentage of each process is given in Fig.19, whereas the time to complete PDE one cycle is given in Fig.20: Note that none of the times required for all process in one cycle (combustion, exhaust and fuel injection) depend PDE length. Moreover, the one cycle time can be estimated, if the PDE length and reservoir pressure P_r are both given; it is closely proportional to PDE length.

The thrust density of each Model PDE (Cases(a)~(d)) is given in Fig.21, showing that

it is again irrelevant to PDE length; a fixed thrust density is essentially obtained. In general, as mentioned above, the performance of Model PDE has no dependence on PDE length, but depends on (1) the initial conditions, (2) intake ports width and (3) reservoir pressure P_r .

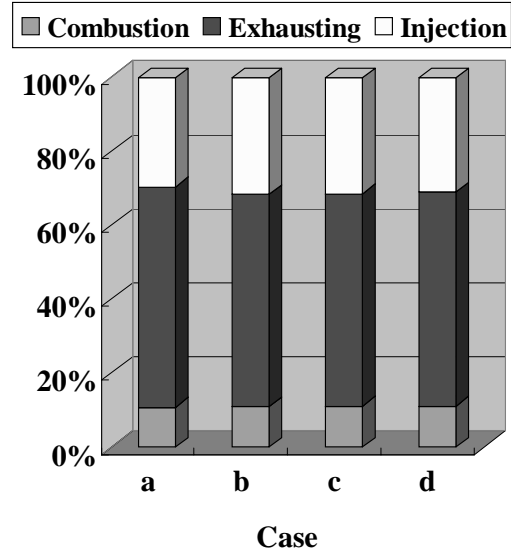


Fig. 19: Percentage of each process for 4 Model PDEs (Cases(a)~(d))

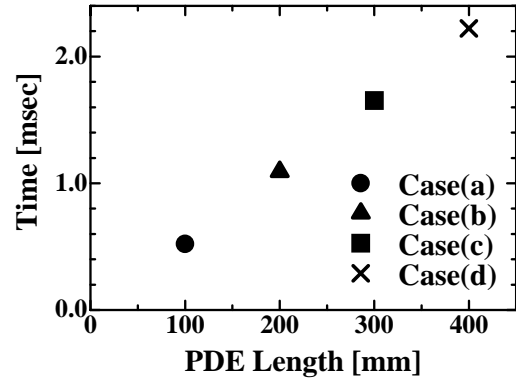


Fig. 20: Time needed for one cycle of Model PDEs (Cases(a)~(d))

Conclusions

In this study, a 2-dimensional analysis of PDE two-cycle operation is performed for 4 different PDE lengths, where we pay attention specifically to the behaviors of (1) burnt gase exhaust and (2) oxyhydrogen injection during the 2nd cycle.

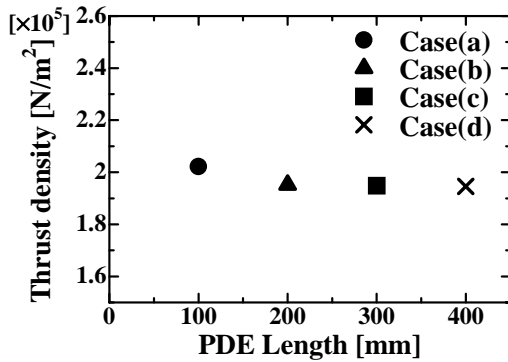


Fig. 21: Thrust density of 4 Model PDEs (Cases(a)~(d))

- During the 1st cycle, the detonation propagation and subsequent slow pressure relaxation process inside PDE are simulated under the ground condition. It is examined that the flow at PDE exit plane becomes choked during exhaust process where the process behaves as 1-dimensional flow.
- The impulse per unit depth increases in proportion to PDE length L . The impulse from our 2-dimensional analysis gives a nice fitting with a straight line given by Kailasanath 1-D analysis.
- During the 2nd cycle, the injection of oxyhydrogen mixture from intake ports generates expansion and diffusion of fuel.
- When the open ratio (intake port width/ PDE width) becomes smaller, it is found out that the fuel injection time increases sharply. Change of injection angle has not influenced the fuel injection time at all. Thus, the fuel injection time is dependent only on the reservoir pressure and intake port width.
- The time ratios among elementary processes (combustion, exhaust and fuel injection) are irrelevant to PDE length. Moreover, the one cycle completion time can be estimated, if the PDE length and reservoir pressure are both given; the cycle time is closely proportional to PDE length.
- The thrust density which is the most important performance of PDE is nearly independent of PDE length.

References

- [1] S.Eidelman and W.Grossmann: A Review of Propulsion Applications of the Pulsed Detonation Engine Concept, AIAA 89-2446, 1989
- [2] G.Roy: Review of Recent Developments in Combustion and Detonation Research, AIAA 2001-0473, 2001
- [3] V.P.Korobeinikov, V.A.Levin, V.V.Markov and G.G.Chernyi: Propagation of Blast Waves in a Combustible Gas, *Astronautica Acta*, 17(1972), pp.529-537
- [4] E.Oran, T.Young and J.Boris: Application of Time-Dependent Numerical Methods to the Description of Reactive Shocks, Seventeenth Symposium (International) on Combustion (1979), pp.43-54.
- [5] K.Kailasanath: A Review of PDE Research-Performance Estimates, AIAA 2001-0474, 2001
- [6] R.A.Strehlow: *Gas Phase Detonation : Recent Developments*, Combustion and Flame Vol.12, pp.81-101, 1968.
- [7] T.Fujiwara, S.Kawai, T.Miyasaka and F.Y.Zhang: Intermittent Flow Calculation/Experiment in a Single-Pulse Detonation Engine, 18th ICDEERS, 2001
- [8] T.Fujiwara, K.Fukiba and T.Miyasaka: Efficiency Study of PDE Based on Quasi-onedimensional Calculation of Detonation, Chemical Physics Reports, Journal of Russian Academy of Sciences Vol.20, pp.99-104, 2000
- [9] Endo, T. and Fujiwara, T.: A Simplified Analysis on a Pulse Detonation Engine Model, Transactions of the Japan Society for Aeronautical and Space Science. Vol.44, No.146, Feb.(2002).